High-fidelity optical reporting of neuronal electrical activity with an ultrafast fluorescent voltage sensor

François St-Pierre[1,2], Jesse D Marshall[3,4], Ying Yang[1,2], Yiyang Gong[3,4], Mark J Schnitzer[3–5] & Michael Z Lin[1,2]

Accurate optical reporting of electrical activity in genetically defined neuronal populations is a long-standing goal in neuroscience. We developed Accelerated Sensor of Action Potentials 1 (ASAP1), a voltage sensor design in which a circularly permuted green fluorescent protein is inserted in an extracellular loop of a voltage-sensing domain, rendering fluorescence responsive to membrane potential. ASAP1 demonstrated on and off kinetics of ~2 ms, reliably detected single action potentials and subthreshold potential changes, and tracked trains of action potential waveforms up to 200 Hz in single trials. With a favorable combination of brightness, dynamic range and speed, ASAP1 enables continuous monitoring of membrane potential in neurons at kilohertz frame rates using standard epifluorescence microscopy.

Understanding how information is processed in the brain would benefit from precise spatio-temporal recording of electrical activity in individual neurons and larger neuronal circuits. Genetically encoded fluorescent indicators are promising tools for optical reporting of brain activity, as they allow monitoring of genetically defined neuronal circuits and do not require chemical access. An ideal genetically encoded indicator would produce large fluorescence responses, facilitating spatio-temporal imaging of how input signals are processed by neurons into output responses such as action potentials (APs)[1,2]. An ideal indicator would also have millisecond-timescale kinetics, enabling interrogation of synchrony and temporal coding in individual neurons and across large neuronal populations[3]. In particular, tracking high-frequency firing would be useful for visualizing how bursts of neurotransmission are decoded by postsynaptic neurons[4] and for understanding how the 50–200-Hz firing of fast-spiking interneurons regulates information processing in the brain[5,6] or is affected in disease[7].

A genetically encoded sensor with these capabilities had not previously been developed. After intense engineering efforts, fluorescent protein–based calcium reporters can now detect single APs[8]. However, they do not provide a direct readout of membrane potential changes. Furthermore, given that calcium transients can persist in neurons for hundreds of milliseconds[9], calcium responses cannot track high-frequency AP trains. For example, the responses measured by GCaMP6f, the fastest variant in the latest iteration of calcium sensors, have mean half decay times ($\tau_{1/2}$) of 142 ± 11 ms (1 AP, mouse V1 cortex), 400 ± 41 ms (10 APs, dissociated neuronal cultures) and ~650 ms (zebrafish tectum)[8]. Accurate reporting of neuronal activity would therefore benefit from sensors that more directly report membrane potential.

Existing fluorescent voltage sensors are constructed from one of two types of voltage-sensing proteins: seven-helix microbial rhodopsins and four-helix voltage-sensing domains (VSDs) from voltage-sensitive phosphatases or ion channels. Some rhodopsin-based sensors produce large fluorescence responses in dissociated neuronal cultures, but they are not sufficiently bright to report neuronal activity over background fluorescence in brain slices or *in vivo*[10,11]. In addition, they are still slow compared with the typical 2-ms duration of APs in pyramidal neurons. Finally, their use can be complicated by the dependence of voltage sensitivity on illumination intensity and wavelength, and nonlinear increases in fluorescence with increasing illumination intensity[12]. Voltage sensors using four-helix VSDs are typically brighter than rhodopsin-based sensors, but produce suboptimal fluorescence responses to neuronal activity[13–19], exhibit inactivation kinetics that are too slow for following fast trains of APs[13,15–17,19,20], and/or require excitation at wavelengths below 450 nm, where phototoxicity and autofluorescence are more problematic[17,18]. The recently developed ArcLight sensor produces the largest fluorescence response to APs among previously reported VSD-based sensors and is excited at ~488 nm, but slow kinetics limit its ability to resolve closely spaced spikes, especially when they are superposed on large excitatory postsynaptic potentials[15,18,21]. Thus, no existing genetically encoded activity sensor possesses all of the characteristics needed for accurate optical reporting of neuronal activity *in vivo*. We therefore sought to develop a voltage sensor with sufficient brightness, dynamic range and kinetics for detection of neuronal activity ranging from subthreshold potentials to rapid trains of APs.

RESULTS

The extracellular loop between the third (S3) and fourth (S4) transmembrane segments of VSDs is thought to undergo substantial conformational changes following depolarization[22]. In particular, crystal structures of a VSD isolated from the seasquirt *Ciona intestinalis* voltage-sensitive phosphatase (VSP) suggest that repolarization

[1]Department of Bioengineering, Stanford University, Stanford, California, USA. [2]Department of Pediatrics, Stanford University, Stanford, California, USA. [3]James H. Clark Center, Stanford University, Stanford, California, USA. [4]CNC Program, Stanford University, Palo Alto, California, USA. [5]Howard Hughes Medical Institute, Stanford University, Stanford, California, USA. Correspondence should be addressed to F.S.-P. (stpierre@alum.mit.edu) or M.Z.L. (mzlin@stanford.edu).

Received 16 February; accepted 28 March; published online 22 April 2014; doi:10.1038/nn.3709

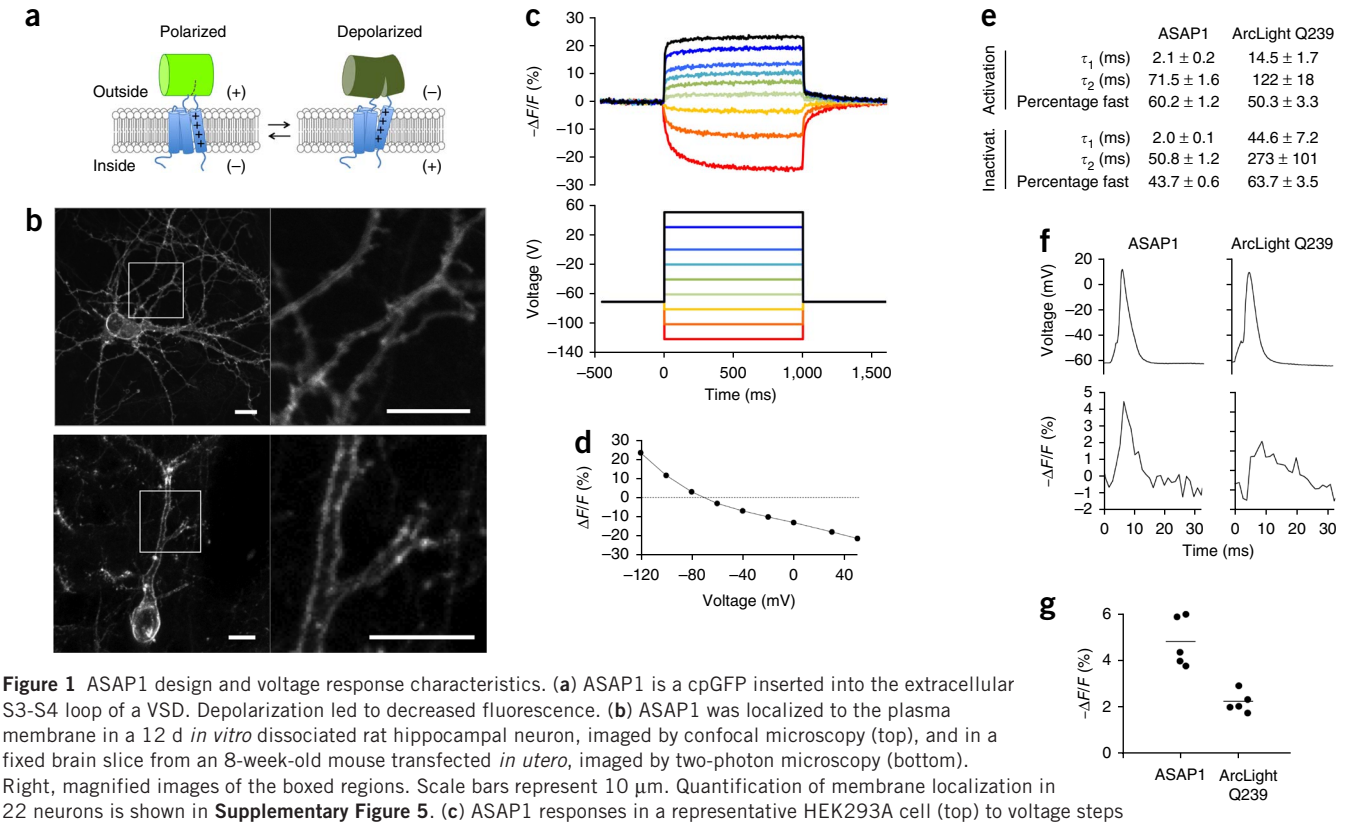

Figure 1 ASAP1 design and voltage response characteristics. (**a**) ASAP1 is a cpGFP inserted into the extracellular S3-S4 loop of a VSD. Depolarization led to decreased fluorescence. (**b**) ASAP1 was localized to the plasma membrane in a 12 d *in vitro* dissociated rat hippocampal neuron, imaged by confocal microscopy (top), and in a fixed brain slice from an 8-week-old mouse transfected *in utero*, imaged by two-photon microscopy (bottom). Right, magnified images of the boxed regions. Scale bars represent 10 µm. Quantification of membrane localization in 22 neurons is shown in **Supplementary Figure 5**. (**c**) ASAP1 responses in a representative HEK293A cell (top) to voltage steps from –120 to 50 mV (bottom). Responses were measured at 5-ms intervals and were normalized to fluorescence at the –70-mV holding potential. (**d**) Mean ASAP1 response to transmembrane voltage in HEK293A cells ($n = 10$ cells). Error bars (s.e.m.) are too small (0.2–1.2% in absolute value) to be easily visible on graph. (**e**) Comparison of activation and inactivation kinetics of ASAP1 ($n = 4$ cells) and ArcLight Q239 ($n = 6$) in HEK293A cells. Data are presented as mean ± s.e.m. (**f**) Comparison of ASAP1 and ArcLight Q239 responses to representative single trial recordings of APs induced by current injection in cultured hippocampal neurons. AP full widths at half-maximum (FWHM) of the voltage traces (top) were 3.3 and 3.6 ms for ASAP1- and ArcLight Q239–expressing neurons, respectively. The corresponding FWHM of the fluorescence responses (bottom) were 3.7 ms and 6.5 ms for ASAP1 and ArcLight Q239, respectively. (**g**) ASAP1 produced larger responses to current-triggered APs in cultured hippocampal neurons than ArcLight Q239 ($P = 0.001$, $n = 5$ neurons from 3 litters for each sensor). Each data point is the average response of an individual neuron over 12–25 APs per neuron (91 APs total for ASAP1 and 87 APs total for ArcLight Q239). For each sensor, the mean response over all tested neurons is depicted using a horizontal bar.

(deactivation) causes upward reorientation of S3-S4 loop residues, partial unwinding of S3 at its extracellular end and disappearance of a short helix in the middle of the S3-S4 loop[23]. We reasoned that insertion of GFP into this location might allow voltage-induced movements to perturb GFP fluorescence. We also hypothesized that circular permutation of GFP, bringing its termini near the chromophore, would enhance conformational coupling between the VSD and fluorescent protein domains. We chose a VSD from the chicken *Gallus gallus* as an initial candidate VSD because it has a shorter S3-S4 loop than *Ciona intestinalis* VSD (**Supplementary Fig. 1a**), which we hypothesized would increase coupling between voltage-induced movements and GFP barrel distortions. We constructed and tested fusions of the circularly permuted GFP (cpGFP) from GCaMP3 (ref. 24) to the S3-S4 loop of the *Gallus gallus* VSD (GgVSD). We included an R153Q mutation that has been shown to shift the voltage response of *Ciona intestinalis* VSPs to a less negative range of potentials[25].

We obtained several protein constructs with cpGFP inserted into GgVSD that were well expressed at the plasma membrane of HEK293A human embryonic kidney cells (**Supplementary Fig. 1b**) and showed a fluorescence decrease in response to membrane depolarization (**Supplementary Fig. 1c**). Beginning with the brightest variant, where cpGFP was inserted between residues 147 and 148 of GgVSD, we tested substitutions of various fluorescent proteins (**Supplementary Fig. 1d**) and found that the OPT variant of circularly permuted superfolder GFP[26] (cpsfGFP-OPT) improved both brightness and dynamic range while maintaining efficient expression at the membrane. We named this protein Accelerated Sensor of Action Potentials 1 (ASAP1; **Fig. 1a**).

We created ASAP1 variants to test whether our initial choice of GgVSD with an R153Q mutation was optimal. Substituting VSDs from *Danio rerio* or *Xenopus laevis* in place of GgVSD in ASAP1 produced voltage sensors with comparable membrane expression, but lowered dynamic range (**Supplementary Fig. 2a**,**b**). Sensors containing the VSD from *Ciona intestinalis* (CiVSD) did not localize well to the plasma membrane (**Supplementary Fig. 2a**). As fusions with fluorescent proteins at either intracellular termini of CiVSD can be well localized at the membrane[13,15,16,18,25], the observed mislocalization appears to be specific to insertion of a fluorescent protein into the extracellular S3-S4 loop rather than an intrinsic property of CiVSD. Reversion of the R153Q mutation did not affect membrane expression of ASAP1, but lowered the fluorescence response to hyperpolarizing signals (**Supplementary Fig. 2a**,**c**).

We next investigated the structural determinants necessary for the voltage sensitivity of ASAP1. Dimming following depolarization suggested that VSD movement disrupts hydrogen-bonding interactions between the beta-barrel and the chromophore that stabilize the deprotonated form of the chromophore. Modifying the circular permutation breakpoint in GFP reduced

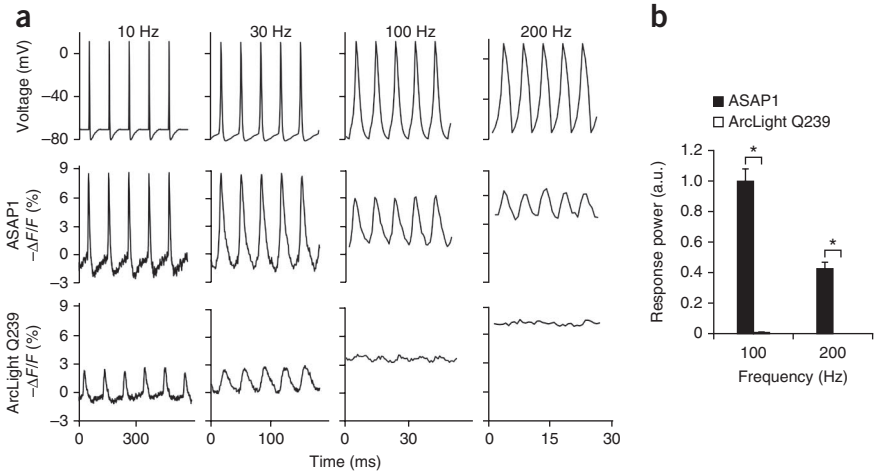

Figure 2 Monitoring simulated AP trains in voltage-clamped HEK293A cells. (**a**) ASAP1 followed 200-Hz trains of AP waveforms, whereas ArcLight Q239 followed trains of 30 Hz, but not 100 or 200 Hz. For each frequency, simulated trains of APs (2.0-ms FWHM, 75-mV peak amplitude) were applied for 1 s. Traces shown are the fluorescence response to 5 AP waveforms at 500 ms from the start of each train. (**b**) Quantification of frequency responses of ASAP1 and ArcLight Q239 to 100-Hz and 200-Hz simulated spike trains. The power spectral density (PSD) of optical responses during spike trains was estimated as the magnitude-squared of the Fourier transform of the fluorescence signal. Amplitudes of the 100-Hz and 200-Hz power peaks for the 100-Hz and 200-Hz spike trains, respectively, were calculated and normalized to ASAP1's mean 100-Hz peak amplitude during 100-Hz trains. Consistent with the example traces shown in **a**, ArcLight Q239 produced little or no response at these frequencies, with mean peak amplitudes of 0.012 ± 0.001 (100 Hz) and <0.001 (200 Hz). ASAP1 showed greater mean response amplitudes to both 100-Hz and 200-Hz simulated AP trains (100 Hz, $P = 0.021$; 200 Hz, $P = 0.031$). Differences are statistically significant (asterisks) following Holm-Bonferroni correction for multiple comparisons. Similar values were obtained using PSDs calculated as the Fourier transform of the autocorrelation function of each optical response. For each train, $n = 5$ HEK293A cells per construct. Error bars represent s.e.m.

the response amplitude; some variants also had inverted responses (**Supplementary Fig. 3a–c**). Removing the first residue of cpsfGFP-OPT (immediately following the S3-GFP junction, Phe145 in the original GFP numbering) severely reduced response. In contrast, removing other amino acids at the GgVSD/cpsfGFP-OPT junction, such as the last residue of cpsfGFP-OPT, had modest effects on dynamic range (**Supplementary Fig. 3d,e**). Certain conservative mutations of Phe145 impaired response (**Supplementary Fig. 4**). Notably, mutation of Phe145 to Tyr markedly reduced dynamic range. This result is consistent with the smaller response amplitude of our initial sensors, which used an alternative cpGFP containing Tyr145 (**Supplementary Fig. 1c**). Our findings suggest that the modulation of cpsfGFP-OPT by voltage is sensitive to the structure near the breakpoint, as previously seen with calcium sensors based on circularly permuted fluorescent proteins[27,28]. In particular, they suggest that cpsfGFP-OPT responds to a conformational change on the S3 side of the linker, consistent with models of VSD structural transitions[23].

We next tested ASAP1 expression in neurons. ASAP1 produced excellent membrane localization in living dissociated hippocampal neurons and fixed brain slices, both at the cell body and in individual dendrites (**Fig. 1b** and **Supplementary Fig. 5**). To determine whether ASAP1 expression altered membrane capacitance, we transfected cultured neurons with 1–4 times the amount of ASAP1 plasmid used in typical fluorescence imaging experiments. Under these conditions, we observed no change in membrane capacitance following ASAP1 expression compared to that in GFP-transfected neurons (**Supplementary Fig. 6**).

We then quantified ASAP1's dynamic range and kinetics. When expressed in HEK293A cells, ASAP1 responded to voltage steps from −120 to 50 mV with a total fluorescence change ($\Delta F/F$) of −36.3 ± 1.6% (mean ± s.e.m.; **Fig. 1c,d**). The response to a 100-mV depolarization from a holding potential of −70 mV was −17.5 ± 1.0% $\Delta F/F$ (**Fig. 1d**), an order of magnitude larger than previous cpGFP-based voltage sensors such as ElectrikPk[14]. ASAP1 also produced large changes to hyperpolarizing signals, with $\Delta F/F$ of 11.7 ± 0.6%

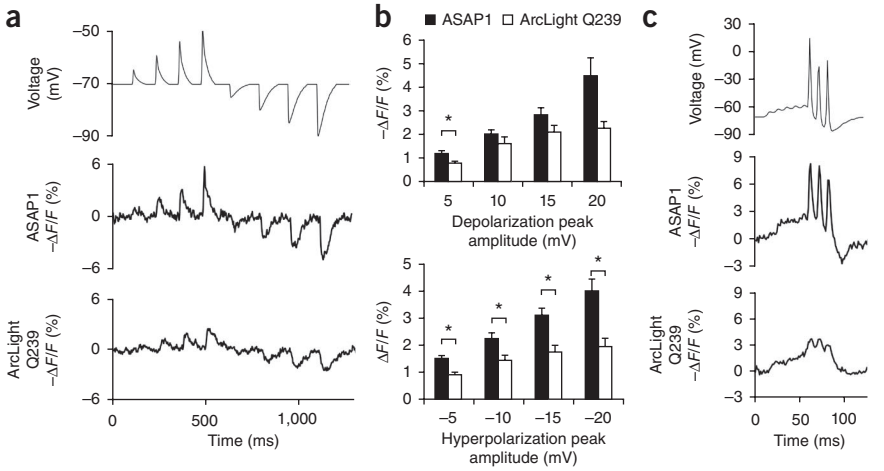

Figure 3 Monitoring simulated hyperpolarizations and subthreshold potentials in voltage-clamped neurons. (**a**) ASAP1 can detect subthreshold potential and hyperpolarization waveforms in cultured hippocampal neurons. Subthreshold depolarizations and hyperpolarizations had peak amplitudes of 5, 10, 15 and 20 mV, and peak FWHM of 17 ms (depolarizations) and 38 ms (hyperpolarizations). (**b**) Quantification of the fluorescence responses to subthreshold depolarizations (top) and hyperpolarizations (bottom). Asterisks identify statistically significant differences from pairwise two-tailed *t* tests adjusted for multiple comparisons using the Holm-Bonferroni method ($P = 0.006$, 5 mV waveform; $P = 0.0005$, 0.008, 0.007 and 0.003 for the –5, –10, –15 and –20-mV waveforms, respectively). Multiple comparisons adjustments were performed separately for depolarizations and hyperpolarizations ($n = 6$ (ASAP1) and 4 (ArcLight Q239) neurons from the same litter). Error bars represent s.e.m. (**c**) ASAP1's faster kinetics allowed improved resolution of a 100-Hz, three-AP waveform sequence in cultured hippocampal neurons. Command voltage spike FWHM is 1.8 ms. Similar observations were made in multiple neurons (ASAP1, $n = 8$ neurons; ArcLight Q239, $n = 6$ neurons; all cells from same litter). Additional examples are shown in **Supplementary Figure 7**.

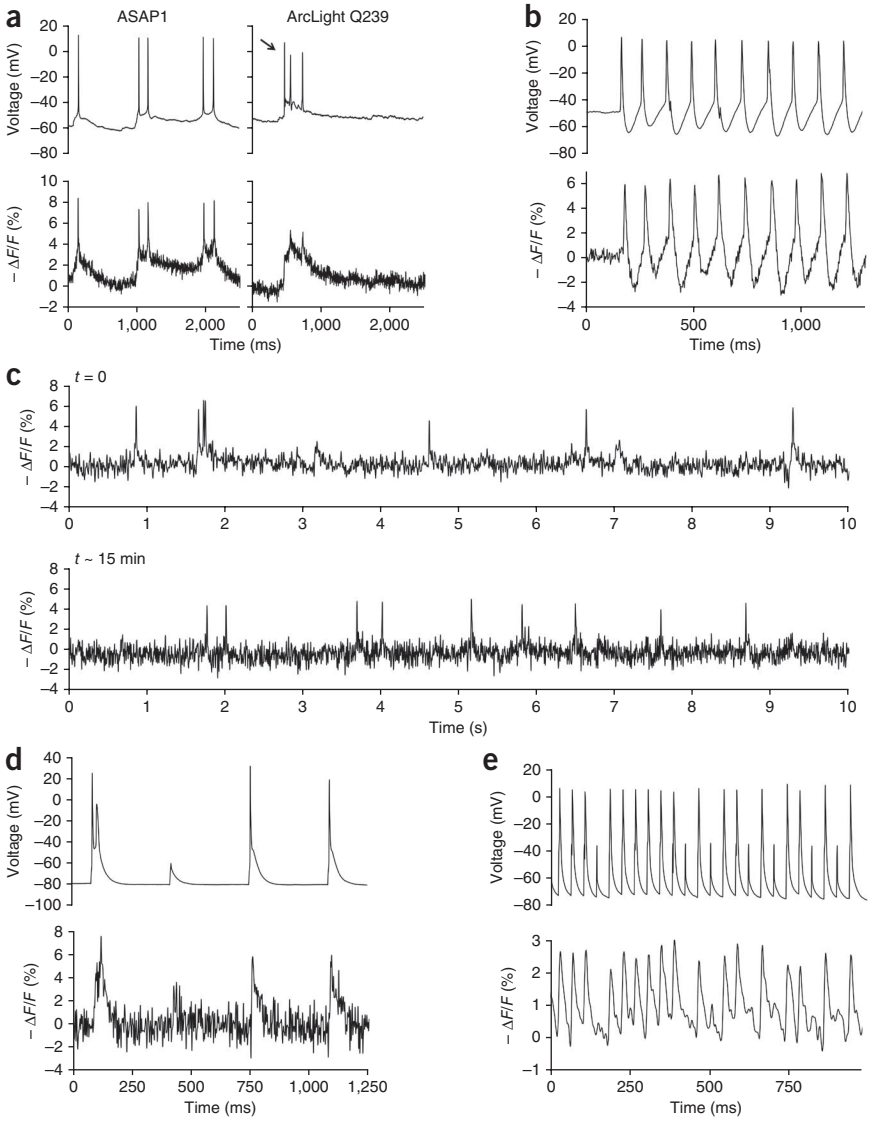

Figure 4 Imaging neural activity in current clamp from cortical slices and dissociated hippocampal cultures. (**a**) Fluorescence responses of ASAP1 (left) and ArcLight Q239 (right) to spontaneous subthreshold potentials and APs in cultured hippocampal neurons. From cell to cell, ASAP1 mean fluorescence responses ranged from −4.8 to −8.1%, averaging −6.3 ± 0.6% (n = 6 neurons from 5 litters, ≥10 APs per neuron). The arrow indicates an AP not detected by ArcLight Q239. Additional examples are shown in **Supplementary Figure 8**. (**b**) ASAP1 followed a spontaneous AP train in a cultured hippocampal neuron ($\Delta F/F$ = −6.2 ± 0.5% mean ± s.e.m., n = 10 APs). Spontaneous bursts are rare events in cultured neurons and we made this observation only a single time in all of our recordings. (**c**) ASAP1 responses to spontaneous activity in a cultured hippocampal neuron at the beginning (top) and end (bottom) of 15 min of continuous illumination (0.036 mW mm^{-2}). Similar observations were made in four neurons from three litters; additional examples are shown in **Supplementary Figure 10**. (**d**) In an acute cortical slice from a mouse brain transfected *in utero*, ASAP1 produced large responses to individual current-induced APs in a layer 5 pyramidal cell ($\Delta F/F$ = −6.2 ± 0.2%, mean ± s.e.m., n = 10 spikes, single observation). (**e**) ASAP1 tracked APs and subthreshold depolarizations in a layer 2/3 neuron injected with current pulses at 25 Hz ($\Delta F/F$ = −1.5 to −3.2%, across 98 APs total from four neurons, each from a different slice from the same animal). All traces are from single trials, without filtering (**a**,**b**,**d**), and with LOWESS smoothing (**c**) or with a 100-Hz fourth order low-pass Butterworth filter (**e**).

and 23.4 ± 0.6% in response to 30 and 50 mV hyperpolarizations, respectively. In HEK293A cells at 22 °C, ASAP1 had rapid biexponential kinetics, with activation and inactivation being characterized by a fast component with time constants of 2.1 ± 0.2 ms and 2.0 ± 0.1 ms, respectively (**Fig. 1e**). The fast component accounted for 60.2 ± 1.2% and 43.7 ± 0.6% of the full activation and deactivation kinetics, respectively. For comparison, we characterized ArcLight Q239, the voltage sensor with the largest fluorescence response to APs of all previous VSD-based sensors. The fast components of the ASAP1 response for activation and inactivation were 7.0 (P = 0.00063) and 22.5 (P = 0.002) times as fast as those of ArcLight Q239, respectively, whereas the slow components were 1.7 (P = 0.034) and 5.4 (P = 0.0095, two-tail Mann-Whitney U test) times as fast.

We predicted that ASAP1's faster kinetics compared with ArcLight Q239 would increase the fidelity by which fluorescence tracks transmembrane voltage and would enhance responses to fast events such as APs. Indeed, although ArcLight Q239 produced a broad fluorescence trace in response to single APs in cultured hippocampal neurons, as previously reported[15], the fluorescence response of ASAP1 to single APs more closely resembled the corresponding voltage response (**Fig. 1f**). Averaging over the entire cell body, ASAP1 produced a fluorescence response of −4.8 ± 0.5%, 2.2 times as large as the −2.2 ± 0.2% response that we observed with Arclight Q239 (**Fig. 1g**). The larger response to single APs with ASAP1 is consistent with its ~7-fold faster on (activation) kinetics, which are better matched to the kinetics of APs.

We next tested the ability of ASAP1 to track various membrane potential waveforms. In voltage-clamped HEK293A cells, ASAP1 was able to track spike trains of up to 200 Hz while clearly discerning individual peaks in single trials without filtering. In contrast, ArcLight Q239 traces at 100 Hz appeared to be flattened with an elevated baseline and poor peak discrimination (**Fig. 2a**,**b**). In cultured hippocampal pyramidal neurons, ASAP1 was able to detect subthreshold depolarizations in the form of simulated excitatory postsynaptic potentials (EPSPs) and inhibitory postsynaptic potentials of 5–20-mV amplitude, comparing favorably with ArcLight Q239 (**Fig. 3a**,**b**). Notably, ASAP1 was able to resolve spikes superimposed on a large compound EPSP, whereas ArcLight Q239 was not (**Fig. 3c** and **Supplementary Fig. 7**). ASAP1 also detected spontaneous spikes, spontaneous ~10-Hz bursting and subthreshold potential changes between spikes in neurons (**Fig. 4a**,**b** and **Supplementary Fig. 8**). As observed previously under voltage clamp (**Fig. 3c**), ArcLight Q239 failed to detect or produced minimal responses to spontaneous APs superposed on large EPSPs (**Fig. 4a** and **Supplementary Fig. 8**). ASAP1 appeared to produce larger fluorescence responses to spontaneous ($\Delta F/F$ = −6.3 ± 0.6%; **Fig. 4a**) than current-induced

($\Delta F/F = -4.8 \pm 0.5\%$; **Fig. 1g**) APs, but this difference was not statistically significant ($P = 0.07$). ASAP1 responses to slow low-amplitude changes were disproportionally larger than to the fast component of APs (**Fig. 4a**); this is expected from the relative steepness of the fluorescence response near the resting potential (**Fig. 1d**) and a slow component in the ASAP1 response (**Fig. 1e**).

To investigate ASAP1's suitability for imaging neuronal activity over longer durations, we first determined its photobleaching time constant in neurons under continuous illumination (0.12 mW mm^{-2} of 470–490-nm light) as 35.0 ± 2.5 min (**Supplementary Fig. 9**). For comparison with probes we developed previously, we estimated the time over which the signal to noise ratio (SNR) for AP detection decays from 4 to 2 as a result of photobleaching at a fixed excitation intensity to be 49.1 ± 9.8 min (mean ± s.e.m., $n = 4$ neurons), longer than voltage sensors based on fluorescence resonance energy transfer (FRET)[16]. As this calculation was based on extrapolations from short recordings, we also directly tested ASAP1's ability to monitor spontaneous neuronal activity over longer durations. We easily detected APs in cultured neurons over 15 min of constant illumination (**Fig. 4c** and **Supplementary Fig. 10**). Peak SNR decreased modestly from 14.6 ± 2.3 to 9.4 ± 1.3 ($n = 4$ neurons from 3 litters; paired t test, $P = 0.047$), partially as a result of a 19.9 ± 5.1% reduction in the AP response (paired t test, $P = 0.014$). The observed increase in baseline noise (23.3 ± 20.5%) did not reach statistical significance (paired t test, $P = 0.34$). These results suggest that ASAP1 has sufficient dynamic range, brightness and photostability for experiments requiring long durations. However, the magnitude of photobleaching and photodamage will likely depend on experimental conditions, such as illumination power, ASAP1 expression levels, neuron type and specimen preparation.

Finally, we investigated ASAP1 performance in acute cortical slices from mouse brains transfected *in utero*. ASAP1 reported current-induced APs in layer 5 pyramidal neurons in single trials without filtering or averaging (**Fig. 4d**) and was able to distinguish between subthreshold depolarizations and APs. ASAP1 also reliably reported current-induced 25-Hz AP trains in layer 2/3 neurons (**Fig. 4e**), detecting all APs and most subthreshold depolarizations. Thus, ASAP1 is able to discriminate between subthreshold voltage changes, single APs and closely spaced APs in neurons in culture and in brain slices.

DISCUSSION

Despite decades of development[29], previous voltage-sensing proteins have limitations hindering their use for high-fidelity recording of neuronal activity. Early sensors consisting of GFP fused to ion channels produce slow or small responses in oocytes[29,30] and no responses in neurons as a result of poor membrane trafficking[31]. More recent sensors, with fluorescent proteins fused to intracellular termini of VSDs from VSPs, show improved membrane localization and can detect voltage changes in neurons. These sensors can be divided into three main classes. In the first, a large change (>10%) in FRET between two fluorescent proteins occurs in response to depolarization, but kinetics are slow ($\tau > 10$ ms)[13,16]. In the second class, represented by ArcLight, depolarization produces a large decrease in fluorescence of a pH-sensitive GFP fused to the VSD C terminus, but also with slow kinetics[15]. In the third class of sensor, the fluorescence of single fluorescent proteins attached to the VSD C terminus can be perturbed by voltage with small dynamic range (<5%) and sometimes with fast ($\tau < 5$ ms) on[14,32] and/or off[32] kinetics.

We designed ASAP1 with a different architecture from previous VSD-based sensors. Instead of attaching fluorescent proteins to intracellular locations in VSDs, we inserted cpGFP in the extracellular S3-S4 loop of a VSD. This location enables direct coupling between conformational changes in the S3-S4 linker and β strand 7 of cpGFP, a strand that interacts with the chromophore to stabilize its deprotonated state. Indeed, the large and rapid responses of ASAP1 indicate that movement of the S4 helix and S3-S4 loop in response to depolarization rapidly modulates protonation of the chromophore.

In conclusion, ASAP1 is distinct from earlier sensors in combining efficient membrane localization, high brightness, large dynamic range and fast kinetics, enabling sensitive detection of a wide repertoire of membrane voltage responses in neurons with standard optical equipment. Separately, two of us (Y.G. and M.S.) are reporting voltage sensors based on FRET between a yellow or orange fluorescent protein and a rhodopsin with voltage-dependent absorption[33]. As there are differences in quantitative performance metrics with ASAP1, their respective suitability in particular experimental settings should be determined empirically. Overall, the improved properties of ASAP1 and these rhodopsin-based sensors advance the field substantially toward imaging fast electrical activity in neural tissue. In particular, ASAP1's fast responses to single APs and ability to track high-frequency trains make ASAP1 an excellent sensor for AP detection and counting, either in unitary events or in rapid trains, whereas its large fluorescence changes near the resting membrane potential make it a sensitive reporter for subthreshold excitatory and inhibitory potentials. ASAP1 should facilitate efforts to map the activity of genetically defined neurons in the brain and decode neuronal communication in time and space[34].

METHODS

Methods and any associated references are available in the online version of the paper.

Accession codes. ASAP1 nucleotide sequence: Genbank KJ598785. ASAP1 expression plasmid (pcDNA3.1/Puro-CAG-ASAP1): Addgene 52519.

Note: Any Supplementary Information and Source Data files are available in the online version of the paper.

ACKNOWLEDGMENTS

We thank the following for providing rats or dissociated neurons: H. Park and Y. Geng (Stanford), M. Hintze and S. Ganesan (Stanford), and C. Ramakrishnan and H. Swanson (Stanford). We also thank X. Ding (Tsinghua University) for assistance with cloning ASAP1 variants with cpsepHluorin A227D, Y. Geng (Stanford) for providing microfluidic chambers, J. Chu (Stanford) for a purified preparation of Clover GFP, V. Pieribone (Yale University) for the generous gift of GgVSD(153Q), DrVSD(R153Q) and XlVSD(R152Q), L. Oltrogge (Stanford) for the generous gift of cpsfGFP-OPT, J. Bant (Stanford) for advice on electrophysiological recordings, and members of the Lin laboratory for comments on the manuscript. This work was supported by DARPA (M.Z.L., M.J.S.), National Science Foundation grant 1134416 (F.S.-P., M.Z.L.), a Stanford Graduate Fellowship (J.D.M.), a Walter V. and Idun Berry Postdoctoral Fellowship (Y.Y.), a Stanford University Bio-X Interdisciplinary Initiatives Project grant (M.Z.L., M.J.S.), the Stanford CNC Program (Y.G., J.D.M., M.J.S.), the Howard Hughes Medical Institute (M.J.S.) and the National Academy of Sciences Keck Futures Initiative (Y.G., J.D.M., M.J.S.). M.Z.L. receives funding from the Rita Allen Foundation.

AUTHOR CONTRIBUTIONS

M.Z.L. conceived the study. F.S.-P. and M.Z.L. designed ASAP1. F.S.-P., J.D.M., Y.Y. and Y.G. designed and performed experiments, and analyzed data. M.Z.L. and M.J.S. provided ideas and advice. F.S.-P. and M.Z.L. wrote the manuscript.

COMPETING FINANCIAL INTERESTS

The authors declare competing financial interests: details are available in the online version of the paper.

1. Magee, J.C. Dendritic integration of excitatory synaptic input. *Nat. Rev. Neurosci.* **1**, 181–190 (2000).
2. Zecevic, D. *et al.* Imaging nervous system activity with voltage-sensitive dyes. *Curr. Protoc. Neurosci.* **6**, Unit 6.17 (2003).
3. Castro-Alamancos, M.A. Cortical up and activated states: implications for sensory information processing. *Neuroscientist* **15**, 625–634 (2009).
4. Branco, T. & Hausser, M. Synaptic integration gradients in single cortical pyramidal cell dendrites. *Neuron* **69**, 885–892 (2011).
5. Puig, M.V., Ushimaru, M. & Kawaguchi, Y. Two distinct activity patterns of fast-spiking interneurons during neocortical UP states. *Proc. Natl. Acad. Sci. USA* **105**, 8428–8433 (2008).
6. Royer, S. *et al.* Control of timing, rate and bursts of hippocampal place cells by dendritic and somatic inhibition. *Nat. Neurosci.* **15**, 769–775 (2012).
7. Zhou, F.W. & Roper, S.N. Altered firing rates and patterns in interneurons in experimental cortical dysplasia. *Cereb. Cortex* **21**, 1645–1658 (2011).
8. Chen, T.W. *et al.* Ultrasensitive fluorescent proteins for imaging neuronal activity. *Nature* **499**, 295–300 (2013).
9. Murthy, V.N., Sejnowski, T.J. & Stevens, C.F. Dynamics of dendritic calcium transients evoked by quantal release at excitatory hippocampal synapses. *Proc. Natl. Acad. Sci. USA* **97**, 901–906 (2000).
10. Kralj, J.M., Douglass, A.D., Hochbaum, D.R., Maclaurin, D. & Cohen, A.E. Optical recording of action potentials in mammalian neurons using a microbial rhodopsin. *Nat. Methods* **9**, 90–95 (2012).
11. Gong, Y., Li, J.Z. & Schnitzer, M.J. Enhanced archaerhodopsin fluorescent protein voltage indicators. *PLoS ONE* **8**, e66959 (2013).
12. Maclaurin, D., Venkatachalam, V., Lee, H. & Cohen, A.E. Mechanism of voltage-sensitive fluorescence in a microbial rhodopsin. *Proc. Natl. Acad. Sci. USA* **110**, 5939–5944 (2013).
13. Akemann, W. *et al.* Imaging neural circuit dynamics with a voltage-sensitive fluorescent protein. *J. Neurophysiol.* **108**, 2323–2337 (2012).
14. Barnett, L., Platisa, J., Popovic, M., Pieribone, V.A. & Hughes, T. A fluorescent, genetically encoded voltage probe capable of resolving action potentials. *PLoS ONE* **7**, e43454 (2012).
15. Jin, L. *et al.* Single action potentials and subthreshold electrical events imaged in neurons with a fluorescent protein voltage probe. *Neuron* **75**, 779–785 (2012).
16. Lam, A.J. *et al.* Improving FRET dynamic range with bright green and red fluorescent proteins. *Nat. Methods* **9**, 1005–1012 (2012).
17. Lundby, A., Mutoh, H., Dimitrov, D., Akemann, W. & Knopfel, T. Engineering of a genetically encodable fluorescent voltage sensor exploiting fast Ci-VSP voltage-sensing movements. *PLoS ONE* **3**, e2514 (2008).
18. Tsutsui, H. *et al.* Improved detection of electrical activity with a voltage probe based on a voltage-sensing phosphatase. *J. Physiol.* **591**, 4427–4437 (2013).
19. Gautam, S.G., Perron, A., Mutoh, H. & Knopfel, T. Exploration of fluorescent protein voltage probes based on circularly permuted fluorescent proteins. *Front. Neuroeng.* **2**, 14 (2009).
20. Staff, N.P., Jung, H.Y., Thiagarajan, T., Yao, M. & Spruston, N. Resting and active properties of pyramidal neurons in subiculum and CA1 of rat hippocampus. *J. Neurophysiol.* **84**, 2398–2408 (2000).
21. Cao, G. *et al.* Genetically targeted optical electrophysiology in intact neural circuits. *Cell* **154**, 904–913 (2013).
22. Jensen, M.Ø. *et al.* Mechanism of voltage gating in potassium channels. *Science* **336**, 229–233 (2012).
23. Li, Q. *et al.* Structural mechanism of voltage-dependent gating in an isolated voltage-sensing domain. *Nat. Struct. Mol. Biol.* **21**, 244–252 (2014).
24. Tian, L. *et al.* Imaging neural activity in worms, flies and mice with improved GCaMP calcium indicators. *Nat. Methods* **6**, 875–881 (2009).
25. Dimitrov, D. *et al.* Engineering and characterization of an enhanced fluorescent protein voltage sensor. *PLoS ONE* **2**, e440 (2007).
26. Cabantous, S., Terwilliger, T.C. & Waldo, G.S. Protein tagging and detection with engineered self-assembling fragments of green fluorescent protein. *Nat. Biotechnol.* **23**, 102–107 (2005).
27. Akerboom, J. *et al.* Optimization of a GCaMP calcium indicator for neural activity imaging. *J. Neurosci.* **32**, 13819–13840 (2012).
28. Akerboom, J. *et al.* Genetically encoded calcium indicators for multi-color neural activity imaging and combination with optogenetics. *Front. Mol. Neurosci.* **6**, 2 (2013).
29. Siegel, M.S. & Isacoff, E.Y. A genetically encoded optical probe of membrane voltage. *Neuron* **19**, 735–741 (1997).
30. Ataka, K. & Pieribone, V.A. A genetically targetable fluorescent probe of channel gating with rapid kinetics. *Biophys. J.* **82**, 509–516 (2002).
31. Baker, B.J. *et al.* Three fluorescent protein voltage sensors exhibit low plasma membrane expression in mammalian cells. *J. Neurosci. Methods* **161**, 32–38 (2007).
32. Perron, A., Mutoh, H., Launey, T. & Knopfel, T. Red-shifted voltage-sensitive fluorescent proteins. *Chem. Biol.* **16**, 1268–1277 (2009).
33. Gong, Y., Wagner, M.J., Li, J.Z. & Schnitzer, M.J. Imaging neural spiking in brain tissue using FRET-opsin protein voltage sensors. *Nat. Commun.* advance online publication, doi:10.1038/ncomms4674 (22 April 2014).
34. Knöpfel, T. Genetically encoded optical indicators for the analysis of neuronal circuits. *Nat. Rev. Neurosci.* **13**, 687–700 (2012).

ONLINE METHODS

Plasmid construction. Plasmids were constructed by standard molecular biology methods and verified by sequencing of all cloned fragments. ASAP1 expression plasmid and its complete sequence can be obtained via Addgene (plasmid 52519, www.addgene.org/52519).

We constructed or obtained four circularly permuted fluorescent proteins for use in voltage sensor variants (**Supplementary Fig. 1b**,**d**). First, we constructed a circularly permuted GFP from GCaMP3 by inserting amino acids 145-148 (YNSH) of EGFP to the N terminus of cpGFP149-144 from plasmid pEGFP-N1-GCaMP3 (Addgene 22692)[24]. Second, we designed a circularly permuted Clover[16] GFP by alignment to cpGFP from GCaMP3, creating new termini at original amino acid positions 145 and 144, and linking its original N- and C- termini using the peptide 'GGTGGS' between the C-terminal lysine (K239) and the original starting methionine. Third, we obtained cpsfGFP-OPT145-144 (abbreviated as cpsfGFP-OPT) from L. Oltrogge (Stanford). cpsfGFP-OPT is a circular permutant of a superfolder GFP variant; it was evolved for use in a split GFP system, and contains seven mutations (GFP1-10 OPT mutations) not present in the original superfolder GFP[35]. The full sequence of cpsfGFP-OPT is provided as part of ASAP1. Finally, we designed circularly permuted superecliptic pHluorinA227D[15] (cpsepHluorinA227D) by alignment to cpsfGFP-OPT, creating new termini at original amino acid positions 145 and 144, and linking its original N- and C- termini using the peptide GTGGSAS between the C-terminal lysine (K239) and a lysine originally present near its N terminus (K4).

We constructed ASAP1 using the voltage-sensing domain (VSD) from the *Gallus gallus* voltage-sensitive phosphatase (VSP, GenBank, XP_417079). ASAP1 variants with alternate VSDs were constructed by inserting cpsfGFP-OPT immediately after amino acids G146 (*Xenopus laevis* VSP 2, GenBank, JF440218), amino acid G147 (*Danio rerio* VSD, GenBank, NM_001025458) or amino acids L203 to G214 (*Ciona intestinalis* VSD, GenBank, AB183035). In each case, we isolated the VSD from the VSP by truncating the C-terminus at homologous positions: T183 (*G. gallus*), T182 (*X. laevis*), T183 (*D. rerio*) or S244 (*C. intestinalis*). Besides the R153Q mutation discussed in the text, our VSDs (generous gift of V. Pieribone, Yale University) differ from the corresponding GenBank sequences as follows. First, *G. gallus*, *X. laevis* and *D. rerio* all contain an extra codon (GAG, glutamic acid) after the starting methionine, possibly to match expression levels of *C. intestinalis* VSD, whose wild-type sequence contains this codon. Second, our *G. gallus* has a lysine rather than glutamic acid at amino acid position 14, while *D. rerio* has a proline rather than leucine at position 90; the effect of these differences in sequence has not been carefully examined.

ArcLight Q239 (ref. 15) and ASAP1 variants were cloned between the NheI-HindIII sites of pcDNA3.1/Puro-CAG[16]. All variants contain identical Kozak sequences. To evaluate sensor brightness or membrane localization, we coexpressed sensors with a fusion of mCherry with a farnesylation motif (CAAX) from the CAG promoter by using the encephalomyocarditis virus internal ribosome entry site (IRES); a schematic of the resulting plasmids is shown in **Supplementary Figure 5a**.

HEK293A cell culture and transfection. HEK293A cells (Life Tech) were maintained in high-glucose Dulbecco's Modified Eagle Medium (DMEM, HyClone) supplemented with 5% fetal bovine serum (FBS, vol/vol, Life Tech) and 2 mM glutamine (Sigma) at 37 °C in air with 5% CO_2. Cells were plated onto glass-bottom 24-well plates (*In vitro* Scientific) for standard imaging, or onto uncoated no. 0 12-mm coverslips (Glaswarenfabrik Karl Hecht GmbH) for patch clamping experiments. Transfections were carried out using FuGene HD (Promega) according to manufacturer instructions, except that cells were transfected at ~50% confluence with lower amounts of DNA (200 ng) and transfection reagent (0.6 µl) to reduce cell toxicity. Cells were cultured for ~48 h before experiments were performed.

HEK293A imaging without patch clamping. We used an IX81 microscope with a 60× 1.42-numerical aperture (NA) PlanApo oil-immersion objective (Olympus). Fluorescence excitation was delivered using a 120-W Mercury vapor short arc lamp (X-Cite 120PC, Exfo) through a 485/22-nm (GFP) or 545/30-nm (RFP) filter. Fluorescence emission was passed through a 540/40-nm (GFP) or 605/50-nm (RFP) filter, and recorded using an Orca ER CCD (Hamamatsu) with Micro-Manager[36] software. Fluorescence images shown in **Supplementary Figures 1–4** are representative images selected out of multiple fields of view.

Simultaneous patch clamping and imaging of HEK293A cells. We performed patch-clamp experiments at 22 °C, using an Axopatch 700B amplifier (Axon Instruments) and borosilicate glass electrodes with resistances of 2.5–5 MΩ. Cells were superfused in a chamber mounted on the stage of an Axiovert 100M inverted microscope with a 40× 1.3-N.A. oil-immersion objective (Zeiss). Fluorescence excitation was delivered using a high-power blue light-emitting diode (LED, UHP-MIC-LED-460, Pryzmatix) through a 472/30-nm filter at a power density of 0.4–5.2 mW mm^{-2} at the sample plane. Fluorescence emission was passed through a 525/50-nm filter, and recorded using either an ORCA-Flash4.0 V2 C11440-22CU (Hamamatsu) scientific CMOS camera (experiments for **Fig. 1c**,**d**), or an iXon 860 electron-multiplied charge-coupled device camera (Andor) cooled to −80 °C (all other experiments). Unless otherwise indicated, step voltage depolarizations were applied to change the membrane potential from a holding voltage of −70 mV to voltages ranging from −120 mV to 50 mV for 0.5–1.0 s. For these voltage steps experiments, we captured images at 200 Hz without binning, and the fluorescence response was measured from pixels at the perimeter of the cell (plasma membrane). For experiments with trains of artificial AP waveforms, we captured images at 827 Hz with 4 × 4 binning, and fluorescence response was measured using pixels from the entire cell. The AP waveform, recorded from a hippocampal neuron, has a FWHM of 2.0 ms and peak amplitude of 75 mV. To measure the kinetics of ASAP1 and ArcLight Q239, we expressed these sensors in HEK293T (Tribioscience) cells. Fluorescence excitation was delivered using a 488-nm diode laser (OBIS, Coherent) through a 469/35-nm filter at 25–50 mW mm^2. Fluorescence emission was passed through a 520/40-nm band-pass filter to a PMM02 photomultiplier tube (Thorlabs) and sampled at 5–10 kHz. Double-exponential models were applied to the rising and falling portions of the imaging trace during command step voltages. For all experiments, fluorescence traces were corrected for photobleaching; electrophysiological data was recorded with Clampex (Molecular Devices) and fluorescence images were acquired with Solis (Andor), HCImage (Hamamatsu) or Micro-Manager[36].

Neuronal cell culture and transfection. Animal experiments were performed in accordance with the rules of the Stanford University Administrative Panel on Laboratory Animal Care. Primary hippocampal neurons were dissected from Sprague-Dawley rats on embryonic day 18 and digested with 10–20 U ml^{-1} papain (Worthington) in Hank's Balanced Salt Solution (HBSS) with 2 U μl^{-1} DNaseI for 25 min at 37 °C. Neurons were then dissociated by gentle trituration in Neurobasal (Life Tech) with 10% FBS. Neurons were plated at 4 × 10^4 cells cm^{-2} on 12-mm no. 0 coverslips (Glaswarenfabrik Karl Hecht GmbH) precoated for 24 h with >300-kDa poly-D-lysine (Sigma) in water. Neurons were cultured overnight at 37 °C in air with 5% CO_2 in Neurobasal with 1 × B27 (Life Tech), 2 mM GlutaMAX (Life Tech) and 10% FBS. The following day, 90% of the medium was replaced with identical medium without FBS. Cytosine β-D-arabinofuranoside (Sigma) was added to 2 µM at 5 d *in vitro* (DIV). Neurons were transfected at 7-10 DIV using calcium phosphate[37]. For each well, we transfected 400 ng of sensor DNA and 1.1 µg of empty pcDNA3.1/Puro-CAG vector.

Confocal imaging of live dissociated neurons. Live neurons were imaged 2 d post-transfection in HBSS supplemented with 10 mM HEPES pH 7.4, 1 × B27, 2 mM GlutaMAX, and 1 mM sodium pyruvate on an IX81 microscope with a FluoView FV1000 laser-scanning confocal unit operated using the FV10-ASW v3.01 software (Olympus). Fluorescence excitation was delivered using a 488-nm laser through a 40× 1.3-NA oil-immersion objective (Olympus). Emission was passed through a 530/40-nm emission filter. A single slice close to the bottom of the neuron was imaged using a 1-Airy pinhole setting. Images shown in **Figure 1b** are representative images selected out of multiple fields of view.

Antibody staining and confocal imaging of fixed dissociated neurons. DIV10 neurons were transfected with a plasmid vector expressing both ASAP1 and mCherry-CAAX (see above and **Supplementary Fig. 5a**) as described above, except that a range of plasmid concentrations was used (0.2–1.6 µg of sensor DNA, supplemented to 1.6 µg total DNA with empty pcDNA3.1/Puro-CAG vector). 4 d post-transfection, neurons were washed in HBSS, fixed for 15 min at 22 °C with 4% paraformaldehyde (wt/vol), and washed three times with HBSS. For preparation of intact (non-permeabilized) neurons, we blocked nonspecific staining by incubating neurons for 30 min in blocking buffer: 5% goat serum (vol/vol, Life Tech) in phosphate-buffered saline (PBS, HyClone/Thermo Scientific);

doi:10.1038/nn.3709

neurons were then washed three times with PBS. Primary antibody staining was performed with a rabbit polyclonal antibody to GFP (ab6556, Abcam, 1:2,000) for 2 h, followed by three washes with PBS. Secondary antibody staining was performed with a goat antibody to rabbit conjugated with Alexa Fluor 633 (AF633) dye (A21071, Life Tech) for 2 h in the dark. Multiple published studies have used ab6556 (ref. 38) and A21071 (ref. 39) for similar applications. Cells were washed once with PBS and twice with PBS + 0.1% Triton X-100 (vol/vol, Amresco) for 20 min each time. All steps were performed at 22 °C. Permeabilized neurons were prepared as above, except that Triton X-100 was added to the blocking and staining solutions to a final concentration of 0.1%; washes were performed identically. Coverslips were mounted using Vectashield HardSet mounting medium (H-1400, Vector Laboratories) supplemented with 0.01% sodium azide (wt/vol). Neurons were imaged using a 40× 1.3-NA oil-immersion objective on an IX81 microscope with a FluoView FV1000 laser-scanning confocal unit operated using the FV10-ASW v3.01 software (Olympus). mCherry-CAAX was imaged with a 559-nm laser and a 603/35-nm emission filter. ASAP1-associated Alexa Fluor 633 was imaged with a 635-nm laser and a 705/100-nm emission filter. Images were acquired using a 1-Airy pinhole setting and filtered with a two-pass Kalman filter. All neurons with visible membrane-localized mCherry-CAAX were selected for analysis. For each neuron and wavelength, a *z* stack from −3 to +3 µm relative to the mid-cell position was acquired, with 0.5-µm vertical spacing between slices. The slice showing the best mCherry-CAAX membrane localization was used for quantifying ASAP1 (AF633) membrane localization; this slice was typically at or close to the mid-cell position. For **Supplementary Figure 5e**, membrane and cytosol regions of interest were hand-drawn using the corresponding mCherry-CAAX image to identify region boundaries.

Simultaneous patch clamping and imaging of dissociated neurons. 2 d post-transfection, cells were patch-clamped at 22 °C using borosilicate glass electrodes with resistances of 3–5 MOhm attached to an Axopatch 700B amplifier (Axon Instruments). Cells were superfused with extracellular solution containing 110 mM NaCl, 26 mM sucrose, 23 mM glucose, 5 mM HEPES-Na, 5 mM KCl, 2.5 mM $CaCl_2$ and 1.3 mM $MgSO_4$, adjusted to pH 7.4. The intracellular (pipette) solution contained 115 mM potassium gluconate, 10 mM HEPES-Na, 10 mM EGTA, 10 mM glucose, 8 mM KCl, 5 mM $MgCl_2$ and 1 mM $CaCl_2$, adjusted to pH 7.4. Cells were imaged using the same microscope, camera, filters and illumination as HEK293A cells (see above). Images were captured at 827 Hz (current-induced APs) or 417 Hz (spontaneous APs) with 4 × 4 binning, and fluorescence response was measured using pixels from the entire cell body. Fluorescence traces were acquired while cells were voltage clamped or current clamped in whole-cell mode. For all experiments, fluorescence traces were corrected for photobleaching. To generate APs, ~800 pA of current was injected for 2 ms. We discarded from future analysis neurons with resting membrane potential greater than −50 mV or membrane resistance lower than 100 MOhm. Electrode voltages and currents were recorded using pClamp (Axon Instruments) and analyzed using custom software written in MATLAB. Voltage traces were corrected for the junction potential *post hoc*. The neuron resting membrane potential was measured at $I = 0$ in current clamp immediately after membrane rupture. Membrane capacitance was determined by pClamp v10 (Molecular Devices) preset routines using the current response to 5-mV square pulses.

Photobleaching and long-term voltage sensing in dissociated neurons. Neurons were cultured and transfected as described above, but were left intact (unpatched). We used an ORCA-Flash4.0 V2 C11440-22CU (Hamamatsu) CMOS camera (**Supplementary Fig. 9**) or an iXon 860 (Andor) electron-multiplied charge-coupled device camera (**Fig. 4c** and **Supplementary Fig. 10**) as described above, except that we used a 480/20-nm excitation filter (Chroma HQ480/20x).

Estimating the concentration of membrane-localized ASAP1 molecules. To obtain a coarse estimate of the number of ASAP1 molecules per μm^2 in dissociated neurons (**Supplementary Fig. 6f**), we first purified a preparation of Clover GFP[16] as previously described[40]. We then determined Clover concentration in our preparation by alkali denaturation[41]. We injected dilutions of our Clover preparation into a custom polydimethylsiloxane (PDMS) microfluidics device[42]. To obtain a correspondence between fluorescence and number of Clover molecules, we imaged channels of 10-µm depth using the microscopy system described above. We adjusted this relationship to measure ASAP1 molecules by factoring the difference in brightness between Clover and cpsfGFP-OPT[43]. We assumed that ASAP1 brightness is equivalent to cpsfGFP-OPT at the brightest point of the $\Delta F/F$ versus V curve (−120 mV; **Fig. 1d**), and then factored in the difference in ASAP1 brightness between −120 mV and the resting membrane potential of approximately −70 mV.

***In utero* electroporation, acute slice preparation and imaging.** Embryos from pregnant CD-1 mice (Charles Rivers) were injected with 1–1.5 µl of 1–2 µg μl^{-1} ASAP1 plasmid DNA in PBS and electroporated using five 10-ms 50–55-V voltage pulses delivered at 1 Hz. At P15–30, electroporated pups were anesthetized with 2% isofluorane (vol/vol), and perfused with a sucrose solution containing 234 mM sucrose, 26 mM $NaHCO_3$, 11 mM glucose, 10 mM $MgSO_4$, 2.5 mM KCl, 1.25 mM NaH_2PO_4, 0.5 mM $CaCl_2$, and continuously bubbled with 95% O_2 and 5% CO_2. 300-µm slices were prepared and allowed to recover for 30 min in bubbled artificial cerebrospinal fluid (ACSF) containing 123 mM NaCl, 26 mM $NaHCO_3$, 11 mM glucose, 3 mM KCl, 2 mM $CaCl_2$, 1 mM $MgCl_2$. Slices were placed in an imaging chamber in a customized BX-51WI fluorescence microscope (Olympus), continuously perfused with ACSF, and visualized under a 20× 1.0-NA objective (Olympus). Cells were illuminated with a stable LED source (Heliophor, 89 North) at a power density of 8 mW mm^{-2} or a 488-nm diode laser (OBIS, Coherent) at a power density of 50 mW mm^{-2}. Layer 5 cortical pyramidal cells expressing ASAP1 were patch clamped, held in current-clamp mode and either monitored for spontaneous spiking or injected with 2- to 5-ms current pulses (600–1,500 pA) to induce single spikes with minimal subthreshold contribution. Fluorescence traces were recorded at 400 Hz by an iXon DU-897 EMCCD camera (Andor). For all experiments, fluorescence traces were corrected for photobleaching.

Data analysis. Peak SNR was defined as the ratio of baseline-subtracted fluorescence intensity changes and the s.d. of the baseline trace in a 500-ms window near the AP, in regions with no apparent hyperpolarizations or subthreshold depolarizations. $T_{4\to2}$ is defined as the time a cell, illuminated so as to obtain an initial SNR of 4, can be imaged before the SNR drops to 2 as previously described[16]. Assuming a reciprocal relation between excitation intensity and photobleaching time, the time to decay from an AP SNR of θ to $\theta/2$ is

$$T_{1/2} = \ln(4) \times SNRC^2 \times \frac{\tau_{off}}{2\theta^2}$$

where τ_{off} is the decay time of the fluorescence transient induced by the spike. The signal-to-noise capacity (SNRC) is a dimensionless measure of a probe's ability to report activity and is defined as the instantaneous peak/noise ratio of a probe integrated over all time. For an single-channel probe, SNRC is defined as $SNRC^2 = (\Delta F/F)^2\, N(t)\, \tau_{PB}$, with $\Delta F/F$ the fractional change in fluorescence to a spike, $N(t)$ the rate of emission, and τ_{PB} the photobleaching time constant. We used fluorescence traces from stimulated APs in dissociated neurons to extract the SNRC and τ_{off} (see above).

Statistical methods. Results presented in the form $x \pm y$ represent the mean ± s.e.m., unless indicated otherwise. Statistical comparisons of pre-identified measures of interest between two data sets were performed with the Student *t* test unless otherwise indicated. Prior to performing such statistical comparisons, the Shapiro-Wilk method was used to test the null hypothesis that the data followed a Gaussian (normal) distribution. When this normality hypothesis could not be rejected, Student *t* tests were performed; otherwise, the Mann-Whitney *U* nonparametric test was used. Prior to performing *t* tests, we also tested the null hypothesis of equal variance between the two data sets, and employed Welch's correction when the null hypothesis was rejected. Two-tailed tests were performed at significance level (α) of 0.05. Statistical tests were performed in Excel (Microsoft) and MATLAB (MathWorks). Except where otherwise indicated, neurons for a given experiment were from the same preparation of hippocampal neurons obtained from dissection of rats from the same litter. No statistical methods were used to predetermine sample sizes, but our sample sizes are similar to those generally employed in the field. Data collection and analysis were not

performed blind to the conditions of the experiments. However, as mentioned earlier, we chose cells for data collection and analysis using predefined selection criteria. Furthermore, data analysis was largely performed using automated Matlab and ImageJ routines.

A **Supplementary Methods Checklist** is available

35. Pédelacq, J.D., Cabantous, S., Tran, T., Terwilliger, T.C. & Waldo, G.S. Engineering and characterization of a superfolder green fluorescent protein. *Nat. Biotechnol.* **24**, 79–88 (2006).
36. Edelstein, A., Amodaj, N., Hoover, K., Vale, R. & Stuurman, N. Computer control of microscopes using microManager. *Curr Protoc Mol Biol* **14**, Unit 14.20 (2010).
37. Jiang, M. & Chen, G. High Ca^{2+}-phosphate transfection efficiency in low-density neuronal cultures. *Nat. Protoc.* **1**, 695–700 (2006).
38. Watkins, R.J. *et al.* A novel interaction between FRMD7 and CASK: evidence for a causal role in idiopathic infantile nystagmus. *Hum. Mol. Genet.* **22**, 2105–2118 (2013).
39. Wouterlood, F.G., Boekel, A.J., Kajiwara, R. & Belien, J.A. Counting contacts between neurons in 3D in confocal laser scanning images. *J. Neurosci. Methods* **171**, 296–308 (2008).
40. Lin, M.Z. *et al.* Autofluorescent proteins with excitation in the optical window for intravital imaging in mammals. *Chem. Biol.* **16**, 1169–1179 (2009).
41. Shcherbo, D. *et al.* Bright far-red fluorescent protein for whole-body imaging. *Nat. Methods* **4**, 741–746 (2007).
42. Butko, M.T. *et al.* Fluorescent and photo-oxidizing TimeSTAMP tags track protein fates in light and electron microscopy. *Nat. Neurosci.* **15**, 1742–1751 (2012).
43. Huang, Y.M. & Bystroff, C. Complementation and reconstitution of fluorescence from circularly permuted and truncated green fluorescent protein. *Biochemistry* **48**, 929–940 (2009).

doi:10.1038/nn.3709